Assessment of the plasma start-up in Wendelstein 7-X with neutral beam injection

D. Gradic[1], A. Dinklage[1], R. Brakel[1], P. McNeely[1], M. Osakabe[2], N. Rust[1], R. Wolf[1], the W7-X Team‡ and the LHD Experimental Group[2]

[1] *Max-Planck-Institut für Plasmaphysik, Teilinstitut Greifswald, D-17491 Greifswald, Germany*

[2] *National Institute for Fusion Science, Oroshi, Toki, Japan*

E-mail: dgradic@ipp.mpg.de

Abstract. Plasma start-up by neutral beam injection was investigated for stellarators. A 0-dimensional collisional model was extended to evaluate the temporal evolution of the plasma start-up in a confining toroidal magnetic field. Inclusion of different beam energy components indicated a substantial effect due to the energy dependence of beam-gas collisions. Additional collision processes and particle equations were considered to simulate the plasma start-up in helium-hydrogen mixtures. The isotope effect between operation with hydrogen and deuterium beams was also investigated.

As a major objective the conditions necessary for a plasma start-up with neutral beams in W7-X have been examined. The assessed beam configuration in W7-X was found not to allow plasma start-up by neutral beam injection alone. The model has been validated for experimental data from W7-AS and LHD. Quantitative predictions of this study show that the ratio of the beam-plasma interaction length and the plasma volume is an essential quantity for the successful plasma start-up with neutral beams.

PACS numbers: 52.50.-b, 52.50.Gj, 52.40.Mj, 52.25.Jm, 52.55.Hc, 52.55.Dy

Keywords: neutral beam injection, plasma start-up, Wendelstein 7-X

‡ See author list in Bosch H.-S. *et al* 2013 *Nucl. Fusion* **53** 126001 (16pp)

1. Introduction

Plasma start-up in neutral gases is a necessary step for the initiation of fusion plasma generation in magnetic confinement experiments. Here we focus on plasma start-up in heliotrons or stellarators. Microwaves and fast particles can be employed for plasma start-up in these devices. The stellarator magnetic field is generated predominantly by coils outside the plasma, thus enabling confining vacuum magnetic fields before plasma operation. During plasma start-up, the produced charged particles remain in the confinement volume to effectively sustain the plasma generation.

Electron cyclotron resonance heating (ECRH) has been proven to be a reliable method to generate plasmas in stellarators ([1], [2]). However, varying the magnetic field in some way is common in those experiments, e.g. relevant for B-field scans or high-β investigations. Therefore, the start-up by heating methods not resonant to specific magnetic fields is a valuable extension in experimental capabilities of stellarators. This research was conducted to investigate whether neutral beam injection (NBI) is an alternative for plasma start-up in W7-X to non-resonant ECRH. Neutral beam particles interact with plasma or neutral gas by atomic collisions and this interaction is independent of the applied magnetic field strength. With energies of several tens of keV, the neutral beam particles ionize the neutral target gas or become ionized themselves. The ionized beam fraction provides heat to all target particle species until being thermalized or lost by charge exchange. However, plasma start-up by NBI requires an optimum but low neutral gas density for reasons explained in section 3.7. In combination with the short beam-plasma interaction length in W7-X (due to accessibility reasons), a high shinethrough of the neutral beam is expected during plasma start-up. For one beam line equipped with two neutral beam sources in a low neutral gas environment, a thermal power density of nearly $40\,\mathrm{MW/m^2}$ has been calculated [3] on the inner wall opposite to the neutral beam injector. Although this part of the wall is actively cooled, the heat flux exceeds significantly the cooling capacity of the tiles ($10\,\mathrm{MW/m^2}$) and results in maximum pulse lengths of 400 ms. Plasma start-up by NBI has to be achieved in less time. A specific motivation of this work is therefore to assess if NBI start-up (in a given but unfavorable geometry) can be achieved in W7-X without damaging the structure of the experiment.

The usual technical approach of plasma start-up in stellarators relies on ECRH. Plasma start-up by the exclusive application of NBI has been demonstrated in the stellarator Wendelstein 7-AS [4] (W7-AS) and in the Large Helical Device [5] (LHD). Very recently, direct NBI plasma start-up was achieved in the TJ-II stellarator with lithium-coated walls [6]. NBI plasma start-up assisted by 2.45 GHz microwaves has been accomplished in Heliotron J [7].
For the description of the plasma start-up with neutral beams, 0-dimensional models have been developed by Ott [8] and Kaneko [9]. These models consist of a set of coupled

rate equations to evaluate the involved particle densities and the electron temperature as a function of time. The authors pointed out that fast-beam ions and low temperature plasma electrons play a vital role for the plasma start-up with neutral beams. The plasma start-up phase is initiated when the electrons participate in the ionization process of the neutral background gas. Generally, this is the case for an electron density in the order of the neutral gas density and an electron temperature of several eV such that the generated background plasma gets ionizing ([10]). The specific interaction of elementary processes, such as ionization and electron cooling, depends on the target and NBI gas. Consequently, plasma start-up in a helium target gas was investigated in this study, where the neutral background gas may be any combination of helium and hydrogen. In helium targets, electron cooling is expected to be smaller because of the lack of dissociative processes. Moreover, there is no dissociative recombination in helium.

The 0-dimensional model for this paper is based on the models by [9] and [8]. Early simulations indicated the start-up time in W7-X to be considerably longer than in W7-AS or LHD, for reasons explained in section 4.3. Therefore, the model was extended in several ways to improve the accuracy of the simulations. The following extensions were made:

(i) consideration of the three individual beam energy species that are typically present in neutral hydrogen beams generated with positive ion sources (as e.g. in W7-AS and W7-X). The beam energy species result from the acceleration of H^+, H_2^+ and H_3^+ species in the ion source ([11]).

(ii) consideration of an H_2^+ electron cooling rate and a confinement time, τ_f, for the ionized beam particles

(iii) additional helium particle balances to evaluate a start-up in a helium target gas or in a helium-hydrogen admixture.

(iv) adjustment of the model to simulate either deuterium or hydrogen beams.

As in [8], molecular hydrogen species and dissociative processes are considered for the plasma start-up. Impurities were not included for this research. Therefore, all plasma start-up simulations presented are only valid for negligible impurity concentrations.

In the following section, the rate equations of the plasma start-up model are presented in detail. In the next chapter, the simulations for W7-X are presented, followed by a validation of the model with W7-AS and LHD experimental data.

2. Model for neutral beam driven plasma start-up in W7-X

Plasma start-up with fast neutral beams has been described successfully by 0-dimensional collisional models [9], [8]. In stellarators, it is possible to formulate these models time-dependent on atomic collision processes only. This is because there is no ohmic heating as in tokamaks. Other aspects simplifying a plasma generation model in

stellarators are closed magnetic flux surfaces and a steady magnetic field configuration throughout the start-up phase. This is why processes like transport or the magnetic field configuration can be included by constant parameters such as the ion-confinement times, τ, or the beam-plasma interaction length, l, (see Figure 1). For tokamak start-ups, time-dependent transport losses would need to be considered [12].
A schematic overview of some parameters and the particle species considered in the W7-X model is shown in Figure 1. The W7-X neutral beam injector has a positive ion source generating three beam energy species E_0, $E_0/2$ and $E_0/3$. In the device, the neutral background species (H_2 and He) are homogeneously distributed in the entire vessel volume, V_v, whereas the ions from the beam (H_f^+) and the background (H_2^+, H^+, He^+, He^{2+}) as well as the electrons (e^-) are only present in the confinement volume considered to resemble approximately the later plasma volume, V_p. Concerning the electrons, the population coming from the ionization of the fast beam neutrals is orders of magnitude smaller than the amount coming from the ionization of the background gas. This is why the electron population from the beam ionization is neglected in the electron density rate equation and in the electron energy balance. In the following subsections, the generation and loss processes of each particle species are explained. A detailed parameter list can be found in Table 1 (section 3).

2.1. Fast ion density

When a neutral beam is injected into a low pressure neutral target gas, a small fraction of the beam is ionized by collisions. The ionized beam particles are referred to as fast ions and are denoted with the index f. The fast ions are essential for the plasma start-up with NBI, as the electrons are only heated by collisions with fast ions unless another external heating source is provided.

To determine the fast ion density, the collision cross-sections and the beam-plasma interaction length have to be considered. Along l, fast ions are produced in atomic collision processes. The beam attenuation length, λ_{H^j} is determined by

$$\begin{aligned}\lambda_{H^j}^{-1} = n_e \frac{\left\langle \sigma_{e,H^j}^{ion.} \left| v_{f,H^j} - v_e \right| \right\rangle}{v_{f,H^j}} &+ n_1 \left(\sigma_{1,H^j}^{ion.} + \sigma_{1,H^j}^{cx} \right) \\ &+ n_2 \left(\sigma_{2,H^j}^{ion.} + \sigma_{2,H^j}^{cx} \right) + n_g \sigma_{g,H^j}^{ion.} \\ &+ n_{He} \sigma_{He,H^j}^{ion.} + n_{He^+} \left(\sigma_{He^+,H^j}^{ion.} + \sigma_{He^+,H^j}^{cx} \right) \\ &+ n_{He^{2+}} \sigma_{He^{2+},H^j}^{ion.} \end{aligned} \quad (1)$$

j denotes the beam energy species. (1) and (2) are evaluated separately for each of the three beam energy species. For the model presented in this section, collisions between neutral beam particles H^j and electrons (e), thermal ions (1 = H^+, 2 = H_2^+ and He^+, He^{2+} without notation) and neutrals (g = H_2, He without notation) are considered. For all collisions involving the (thermal) electrons, rate coefficients $\langle \sigma \cdot v \rangle$ are needed for determining the reaction rate. For reactions between the background gas species and

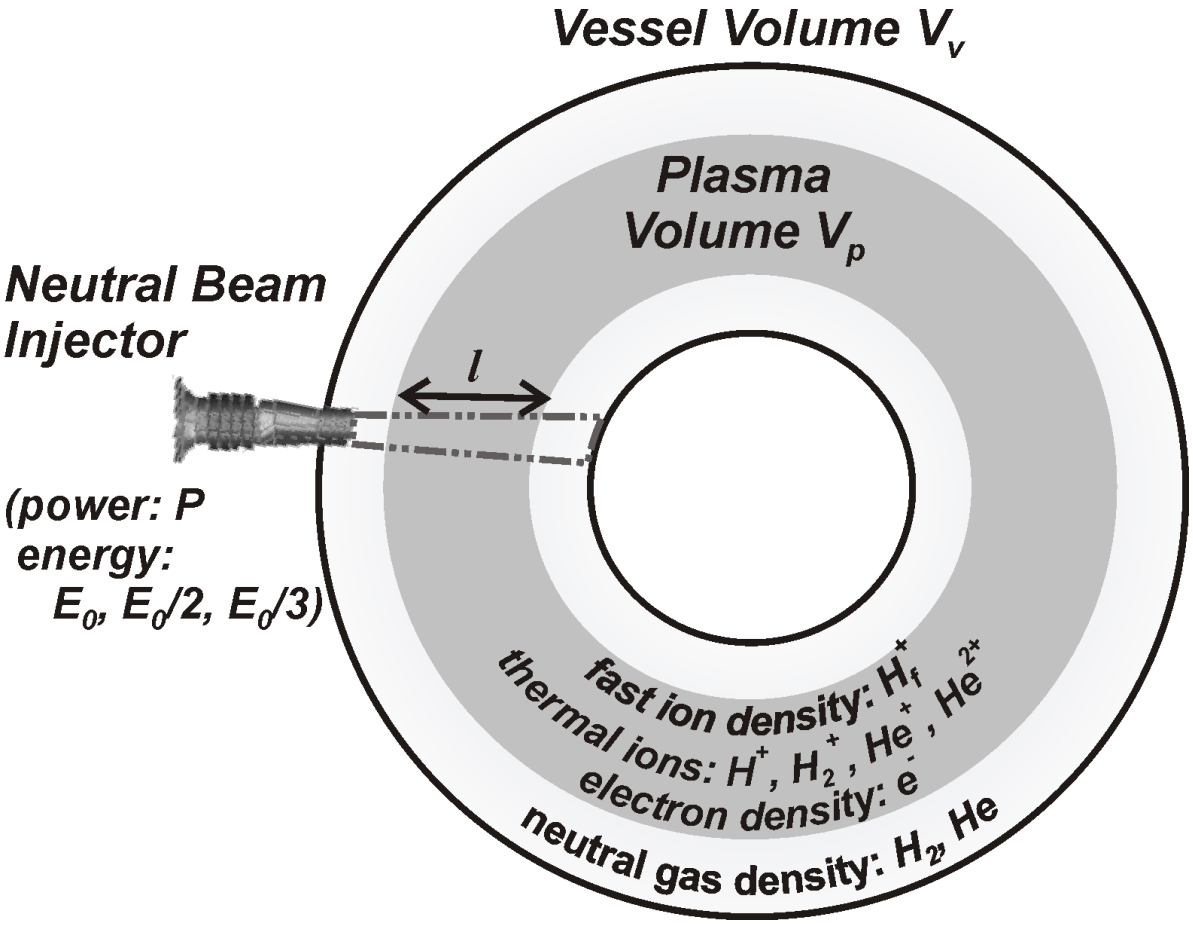

Figure 1. Schematic viewgraph of geometrical considerations and the particle species included in the 0-dimensional plasma start-up model for W7-X.

the three fast mono-energetic beam species, the background particles velocity can be neglected due to their low temperature of a few eV in comparison with the fast beam particles velocity. In this case, the product $\sigma \cdot v_f$ is sufficient. A detailed list of the cross-sections and rate coefficients considered in the model can be found in the Appendix. Given both the number of beam particles entering the interaction volume and the beam attenuation length, the fast ion density can be calculated by

$$\begin{aligned}\frac{\mathrm{d}n_{f,H^j}}{\mathrm{d}t} = &\frac{P}{e \cdot E_j \cdot V_p}\left(1 - \exp\left(-\frac{l}{\lambda_{H^j}}\right)\right) \cdot \frac{p_j}{100} \\ &-n_{f,H^j}\left(n_g \sigma^{cx}_{f,g} + n_{He^+}\sigma^{cx}_{f,He^+}\right. \\ &\left.+n_{He}\sigma^{cx}_{f,He}\right) v_{f,H^j} - \frac{n_{f,H^j}}{\tau_f}\end{aligned} \tag{2}$$

The first term is equivalent to the ionized fraction of the neutral beam. P is beam power, E_j the energy and p_j the power fraction of energy species j in the beam. The generation of fast ions is simulated in the entire plasma volume, V_p, due to the 0-dimensional aspect of the model. As long as the ionized beam particles are not trapped in magnetic wells, they will travel along the magnetic field lines and this assumption will hold. The second

term denotes the losses of fast ions due to charge exchange collisions. The third term considers confinement losses of fast ions in the respective magnetic configuration, with τ_f as the fast particle confinement time.

2.2. Target species

During a plasma-start-up with neutral beam injection, thermal ions are generated by beam-target interaction as well as electron collisions. In neutral hydrogen targets (H_2), the generation of H_2^+ and H^+ involves ionization, dissociation and charge exchange collisions (see tables 7 and 8). The H_2^+ density, denoted by n_2, is determined by

$$\begin{aligned}\frac{\mathrm{d}n_2}{\mathrm{d}t} = n_g \Bigg[& n_e \left\langle \sigma_{e,g}^{ion.} v_e \right\rangle + \sum_{j=1}^{3} \Big(n_{b,H^j} \sigma_{b,g}^{ion.} v_{f,H^j} \\ & + n_{f,H^j} \left(\sigma_{f,g}^{ion.} + \sigma_{f,g}^{cx} \right) v_{f,H^j} \Big) \Bigg] \\ & - n_2 \Bigg[\sum_{j=1}^{3} \left(n_{b,H^j} \sigma_{2,b}^{cx} v_{f,H^j} \right) \\ & + n_e \left(\left\langle \sigma_{e,2}^{rec} \cdot v_e \right\rangle + \left\langle \sigma_{e,2}^{dis} \cdot v_e \right\rangle \right) + \frac{1}{\tau_{th}} \Bigg] \end{aligned} \tag{3}$$

H_2^+ ions are produced by ionization and charge exchange collisions of H_2 with the fast ions and electrons, but they are lost by electron-induced dissociation and dissociative recombination as well as charge exchange with neutral beam particles. A thermal ion-confinement time, τ_{th}, is also considered in Equation (3), simulating losses from the confined volume. τ_{th} is assumed to be the same for all thermal ion species.
The H^+ density is denoted by n_1:

$$\begin{aligned}\frac{\mathrm{d}n_1}{\mathrm{d}t} = n_2 n_e \left\langle \sigma_{e,2}^{dis} \cdot v_e \right\rangle - n_1 \Bigg(& \sum_{j=1}^{3} \left(n_{b,H^j} \sigma_{1,b}^{cx} v_{f,H^j} \right) \\ & + n_e \left\langle \sigma_{e,1}^{rec.} \cdot v_e \right\rangle + \frac{1}{\tau_{th}} \Bigg) \end{aligned} \tag{4}$$

H^+ ions are generated by the dissociation of H_2^+ and lost by radiative recombination and charge exchange processes.
The rate equation for H_2 is determined by the change of the thermal ion density rates (3) and (4). Because the neutral gas is distributed in the entire vessel volume, V_v, the losses of neutral gas have to be restricted to the H_2 particles in the plasma volume, V_p, by the ratio of V_p and V_v:

$$\frac{\mathrm{d}n_g}{\mathrm{d}t} = -\frac{\mathrm{d}\left(n_1/2 + n_2\right)}{\mathrm{d}t} \frac{V_p}{V_v} \tag{5}$$

In the case of a helium target gas, the helium species are determined in a similar way but without dissociative reactions. During the plasma start-up with helium, thermal ions He^+ and He^{2+} are generated:

$$\frac{\mathrm{d}n_{He^+}}{\mathrm{d}t} = n_{He} \Bigg\{ n_e \left\langle \sigma_{e,He}^{ion.} \cdot v_e \right\rangle + \sum_{j=1}^{3} \Big[n_{b,H^j} \sigma_{b,He}^{ion.} v_{f,H^j}$$

$$
\begin{aligned}
&+n_{f,H^j}\left(\sigma^{ion.}_{f,He}+\sigma^{cx}_{f,He}\right)v_{f,H^j}\Big]\Big\}\\
&+n_{He^{2+}}\left[n_e\left\langle\sigma^{rec.}_{e,He^{2+}}\cdot v_e\right\rangle+\sum_{j=1}^{3}n_{b,H^j}\sigma^{cx}_{b,He^{2+}}v_{f,H^j}\right]\\
&-n_{He^{+}}\Big\{n_e\left(\left\langle\sigma^{ion.}_{e,He^{+}}\cdot v_e\right\rangle+\left\langle\sigma^{rec.}_{e,He^{+}}\cdot v_e\right\rangle\right)\\
&+\sum_{j=1}^{3}\Big[n_{b,H^j}\left(\sigma^{cx}_{He^{+},b}+\sigma^{ion.}_{b,He^{+}}\right)v_{f,H^j}\\
&+n_{f,H^j}\sigma^{cx}_{f,He^{+}}v_{f,H^j}\Big]+\frac{1}{\tau_{th}}\Big\}
\end{aligned}
\tag{6}
$$

$$
\begin{aligned}
\frac{\mathrm{d}n_{He^{2+}}}{\mathrm{d}t}=n_{He^{+}}&\left[\sum_{j=1}^{3}n_{f,H^j}\left(\sigma^{ion.}_{f,He^{+}}+\sigma^{cx}_{f,He^{+}}\right)v_{f,H^j}\right.\\
&\left.+n_e\left\langle\sigma^{ion.}_{e,He^{+}}\cdot v_e\right\rangle+\sum_{j=1}^{3}n_{b,H^j}\sigma^{ion.}_{b,He^{+}}v_{f,H^j}\right]\\
&-n_{He^{2+}}\left[\sum_{j=1}^{3}\left(n_{b,H^j}\sigma^{cx}_{b,He^{2+}}v_{f,H^j}\right)\right.\\
&\left.+n_e\left\langle\sigma^{rec.}_{e,He^{2+}}\cdot v_e\right\rangle+\frac{1}{\tau_{th}}\right]
\end{aligned}
\tag{7}
$$

The helium gas density is diminished by all generated thermal helium ions:

$$
\frac{\mathrm{d}n_{He}}{\mathrm{d}t}=-\left(\frac{\mathrm{d}n_{He^{+}}}{\mathrm{d}t}+\frac{\mathrm{d}n_{He^{++}}}{\mathrm{d}t}\right)\frac{V_p}{V_v}
\tag{8}
$$

Similarly to the neutral gas rate equations (5) and (8), the electron density is determined by the change of the ion production rates:

$$
\frac{\mathrm{d}n_e}{\mathrm{d}t}=\frac{\mathrm{d}n_1}{\mathrm{d}t}+\frac{\mathrm{d}n_2}{\mathrm{d}t}+\frac{\mathrm{d}n_{He^{+}}}{\mathrm{d}t}+\frac{\mathrm{d}n_{He^{2+}}}{\mathrm{d}t}
\tag{9}
$$

2.3. Electron energy balance

The electron temperature, T_e, is an important quantity for the plasma start-up, as it strongly impacts the variation of the probability of the electron collisional processes. The change of thermal electron energy $\dot{W}=\frac{\mathrm{d}}{\mathrm{d}t}(n_e k_B T_e)$ is determined by heating and cooling of the electron gas:

$$
\begin{aligned}
\frac{\mathrm{d}(k_B T_e)}{\mathrm{d}t}=&\frac{2/3\cdot e^3\cdot\ln\Lambda}{4\pi\epsilon_0^2 m_e}\sum_{j=1}^{3}\left(\frac{n_{f,H^j}}{v_{f,H^j}}\mathbf{F}(x_{e,j},m_e/m_f)\right)\\
&-2/3\cdot\Big(n_g L_{H_2}(T_e)+n_{H_2^+}L_{H_2^+}(T_e)\\
&+n_{He}L_{He}(T_e)+n_{He^{+}}L_{He^{+}}(T_e)\Big)-\frac{k_B T_e}{n_e}\frac{\mathrm{d}n_e}{\mathrm{d}t}
\end{aligned}
\tag{10}
$$

The first term denotes the heating of electrons by Coulomb collisions with the fast ions. $\ln\Lambda\approx 15$ is the Coulomb logarithm. $\mathbf{F}\left(x_{e,j},\frac{m_e}{m_f}\right)$ is a function expressing the effective heating of the electrons by fast ions (obtained from [14]) and is given by

$$
\mathbf{F}\left(x_{e,j},\frac{m_e}{m_f}\right)=\mathbf{erf}(x_{e,j})-\frac{2x_{e,j}}{\sqrt{\pi}}\left(1+\frac{m_e}{m_f}\right)\exp(-x_{e,j}^2)
\tag{11}
$$

with

$$x_{e,j} = \sqrt{\frac{m_e}{m_f}}\sqrt{\frac{E_j}{T_e}}. \tag{12}$$

The ratio $\frac{E_j}{T_e}$ varies slightly throughout the plasma start-up. Generally, overall heating by fast particles is more effective for small electron temperatures and high fast particle energies, E_j. The next term in Equation (10) is electron cooling by inelastic collisions with cold gas species (H_2, H_2^+, He, He^+). L is the electron cooling rate of the specific particle species. For H_2 and H_2^+ it was determined by

$$L = \sum_i \langle \sigma_i v_e \rangle \, \Delta E_i \tag{13}$$

where $\langle \sigma_i v_e \rangle$ is the reaction coefficient of an inelastic collision i and ΔE_i is the (mean) electron energy loss of the process. As in [8], reactions (2.2.1)-(2.2.8) from [15] were considered for the H_2 cooling rate. The electron cooling rate in H_2^+ was calculated with reactions (2.2.11)-(2.2.14) from [15]. The cooling rates in He and He^+ were obtained from [16]. An overview of all cooling rates is given in Figure 2. For low electron temperatures, the electron cooling rates in hydrogen are considerably higher. This is due to the high rate coefficients of some dissociative processes in hydrogen.

The last term in Equation (10) is cooling by newly ionized electrons contributing to the

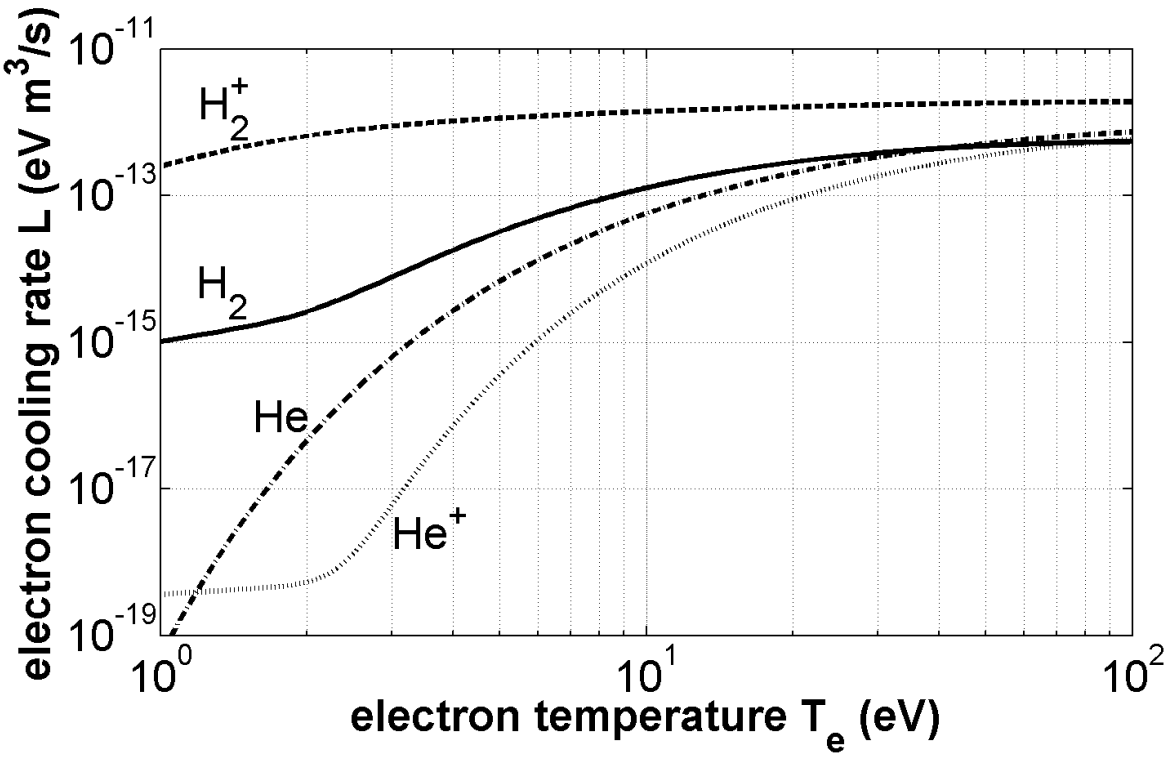

Figure 2. Electron cooling rates in H_2, H_2^+, He and He^+.

electron background. As mentioned earlier, energy losses by impurity radiations, e.g. oxygen or carbon, were neglected for start-up simulations in W7-X. Impurity radiation

losses are considered to have some effect on the simulation results in dependence on their concentration, but as well as a thermal ion temperature, they have not been in the focus of this research. An investigation has been made by [9], where it was found that high impurity contents may prevent plasma start-up due to the large amount of radiative power loss of the electrons.

3. Simulations of NBI plasma start-up in Wendelstein 7-X

3.1. W7-X parameters

The input parameters needed to model the plasma start-up by NBI in W7-X are shown in Table 1. These values are used for all simulations presented in this paper, if not otherwise stated.

Table 1. Standard parameters used for W7-X simulations. The star indicates parameters varied in this study.

interaction length*	l	0.6	m
plasma volume	V_p	30	m^3
vessel volume	V_v	80	m^3
thermal ion-confinement time*	τ_{th}	1	s
fast ion-confinement time*	τ_f	0.1	s
initial electron temperature*	$T_{e,0}$	0.1	eV
neutral gas pressure*	p_{gas}	$5 \cdot 10^{-7}$	mbar
gas temperature	T_{gas}	293	K
beam power (2 sources)	P	3.4	MW
acceleration voltage	U	55	kV
beam species mix	p_j	51:30:19	

In W7-X, the neutral beams will be injected radially into the torus. Thus, the beam-plasma interaction length, $l = 0.6\,\mathrm{m}$, is short compared with other stellarator-type experiments like W7-AS ($l = 2\,\mathrm{m}$) and LHD ($l = 5.6\,\mathrm{m}$). Due to the shinethrough of the neutral beam in plasma start-up conditions, only a beam pulse length of 400 ms or less can be allowed.

Also, due to the radial injection of the neutral beam particles in W7-X, the possibility of Lorentz ionization [17] has been investigated. According to Hiskes [17], Lorentz ionization of excited neutral hydrogen states ($n = 5 \ldots 10$) becomes relevant for electric fields on the order of $E_t = 10^5 \ldots 10^6\,\mathrm{V/cm}$. In W7-X the equivalent electric field would be $E_t \approx 10^4\,\mathrm{V/cm}$ (for $B = 2.5\,\mathrm{T}$ and neutral hydrogen beam particles with a kinetic energy of 55 keV). This field is sufficient for the ionization of $n > 10$ excited states (see [17]). But the $n > 10$ fraction in the neutral beam is not significant, therefore Lorentz ionization has no effect.

There are two ion-confinement times of importance to the model - thermal ion-confinement time, τ_{th}, for the thermalized ions in the plasma of W7-X and the fast ion-confinement time, τ_f, for the ionized beam fraction. Because W7-X is not yet in operation, the values of both ion-confinement times must be estimated. It is expected that there will be a strong dependence of the ion-confinement times on the magnetic field configurations of the machine. Therefore, a variation study of how the plasma start-up time, τ_{psu}, varied with both τ_{th} and τ_f was made (section 3.7). Typical values in the present calculations were chosen to be $\tau_f = 0.1\,\mathrm{s}$ and $\tau_{th} = 1\,\mathrm{s}$.

The initial particle densities considered for (2) - (9) are set to zero, except the neutral gas density. A low pre-ionization degree of the neutral gas in the device due to cosmic and terrestrial radiation has no effect on plasma start-up with NBI. This is demonstrated in another τ_{psu}-variation study in section 3.7.
An initial electron temperature of $T_{e,0} = 0.1\,\mathrm{eV}$ was chosen for the W7-X plasma start-up simulations. From the physical point of view, this may seem odd, but $T_{e,0}$ cannot be chosen as zero in the model due to the definition in (12). Therefore, the smallest electron temperature value defined for the applied rate coefficient data from [15] was taken as the initial value. However, the actual value of the initial electron temperature $T_{e,0}$ does not make a difference with respect to the plasma start-up time τ_{psu} (see next subsection for definition) for $T_{e,0} < 10\,\mathrm{eV}$. This is due to the initial electron density and initial fast ion density value being set to zero (and thus switching off the effects of the electron temperature). The plasma start-up time is not influenced as long as the initial electron temperature is not set greater than $T_e > 10\,\mathrm{eV}$ (for this value the plasma is usually initiated in simulations). If $T_{e,0}$ is chosen below this temperature, its effect on plasma start-up remains small during the simulation and the electron temperature balances very rapidly to a certain temperature level determined by the heating and cooling conditions of (10). (The temporal evolution of the electron temperature and the particle densities is discussed in the next subsection).

For the initial neutral gas pressure, $p_{gas} = 5 \cdot 10^{-7}\,\mathrm{mbar}$ was chosen as a standard value. According to design specifications, the base pressure of W7-X is supposed to be $10^{-8}\,\mathrm{mbar}$. It is not known yet if this base pressure can be achieved in W7-X. For this reason and also to investigate the effect on plasma start-up, a variation of the initial gas pressure was made in section 3.7. The standard value is close to the maximum value for which plasma start-up can be achieved for the set of standard parameters in W7-X.

3.2. W7-X plasma start-up in hydrogen

In Figure 3, the solution of the rate equations for a beam consisting of three energy species is displayed. The simulation is made for a hydrogen (H) beam injected into a pure hydrogen target gas (H_2), starting at $t = 0\,\mathrm{s}$. For reasons of clarity only the total fast ion density is displayed.

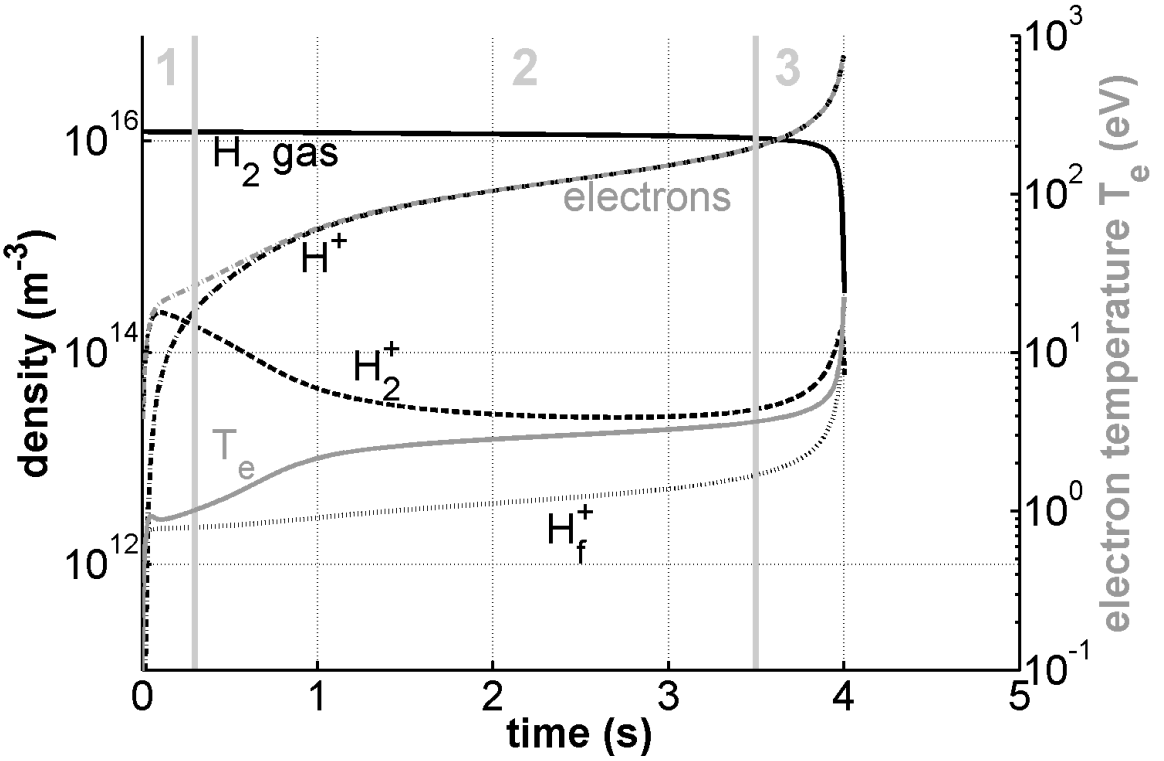

Figure 3. Temporal evolution of particle densities and electron temperature simulated for W7-X plasma start-up conditions (see Table 1). The numbering of the three start-up phases corresponds to the phases as described in the text.

Plasma start-up with neutral beam injection is characteristically developing in different phases.

(i) The phase in the beginning ($t = 0$ ... $t = 0.3\,\mathrm{s}$) is dominated by interaction between the fast beam neutrals and the gas background. Due to the low temperature and density of the electrons, background gas ionization by electrons is considered to be negligible in this phase.

(ii) In the second phase, the particle densities and the electron temperature are slowly changing over time. There is still a large amount of cold neutral target gas, H_2, cooling the electrons and capturing fast ions via charge exchange. At the same time the fast ions moving along the magnetic field lines heat the electrons by Coulomb collisions. The time scale of the second phase is determined by the balance between the energy and particle gain and loss processes. It is noted that in the externally generated confining magnetic field of a stellarator, the efficient energy loss of fast ions is different to tokamaks.

(iii) In the third phase, at $t = 4\,\mathrm{s} = \tau_{psu}$, an avalanche breakdown of the background gas is observed. The breakdown to plasma is characterized by both a strong decrease of the neutral gas density in the plasma volume, while simultaneously the electron temperature and density strongly increase. The breakdown phase is due to the

increase of the electron ionization rate coefficients with T_e and rising electron density. The rate coefficient for ionization by electrons ($\left\langle \sigma_{e,g}^{ion.} \cdot v_e \right\rangle$) increases by more than three orders of magnitude for electron temperatures between 1 and 10 eV (see Figure 13 in Appendix, where the referred rate coefficients are illustrated). In addition, the electron loss rate due to dissociative recombination ($\left\langle \sigma_{e,2}^{rec.} \cdot v_e \right\rangle$) is decreasing for this temperature range. As a result, an increasing fraction of electrons is involved in the ionization process during the breakdown phase. Simultaneously, the decrease of neutral gas density results in less electron cooling by collisions with neutral gas. This in turn leads to a higher growth rate of the electron temperature. Increasing the electron temperature, electron density and decreasing the neutral gas pressure trigger the avalanche breakdown to plasma.

The plasma start-up time, τ_{psu}, denotes the time from the switch on of the beam until breakdown to plasma. There are several possibilities to define the moment of breakdown to plasma. It may be identified by the temporal evolution of the electron temperature, electron density or neutral gas density. Ott [8] investigated several criteria for breakdown, such as $n_e/n_g > 1$, $\mathtt{d}T_e/\mathtt{d}t > 100\,\mathrm{eV\,s^{-1}}$ and $\mathtt{d}(n_e/n_g)/\mathtt{d}t > 100\,\mathrm{s^{-1}}$. All of these criteria were observed to lead to approximately the same start-up time. For this study, $T_e > 15\,\mathrm{eV}$ has been chosen as a secure condition for τ_{psu}, because these temperatures are never achieved when there was no ionization avalanche. An electron temperature $T_e > 15\,\mathrm{eV}$ is only achieved after breakdown to plasma has occurred (independent of the neutral gas species hydrogen or helium). It does not denote a minimum temperature necessary to initiate the plasma. It is not possible to define such a temperature, because both a certain growth rate of the electron density and temperature are necessary conditions for plasma start-up.

3.3. Beam energy resolved simulations

In the NBI system operated for W7-X, a positive ion source is used, resulting in three energy species $E_1 = e \cdot U$, $E_2 = E_1/2$ and $E_3 = E_1/3$ for a given ion acceleration voltage U. In W7-X, the acceleration voltage is planned to be $U = 55\,\mathrm{kV}$, therefore the energy species are $E_1 = e \cdot U = 55\,\mathrm{keV}$, $E_2 = E_1/2 = 27.5\,\mathrm{keV}$ and $E_3 = E_1/3 = 18.3\,\mathrm{keV}$. The power fractions are $p_j = 51 : 30 : 19$ given by experimental findings [13]. By evaluating (1) and (2) for each beam energy species, instead of using an averaged beam energy as in [8], the simulated plasma start-up time is shortened. This is shown in Figure 4, where the temporal evolution of the electron density during the plasma start-up is illustrated. By considering all beam energy species, the simulation gives a plasma start-up time 50% shorter than for a mono-energetic beam with an averaged beam energy $E_{avr.} = \sum_j E_j \cdot p_j = 39.8\,\mathrm{keV}$.

This finding is investigated by a mono-energetic beam assessment, where the neutral beam is assumed to consist entirely of one energy component E_1, E_2 or E_3. For the highest energy component, $E_1 = 55\,\mathrm{keV}$, no plasma start-up is simulated in Figure 4. For the averaged beam energy $E_{avr.} = 39.8\,\mathrm{keV}$ and the lower energy components

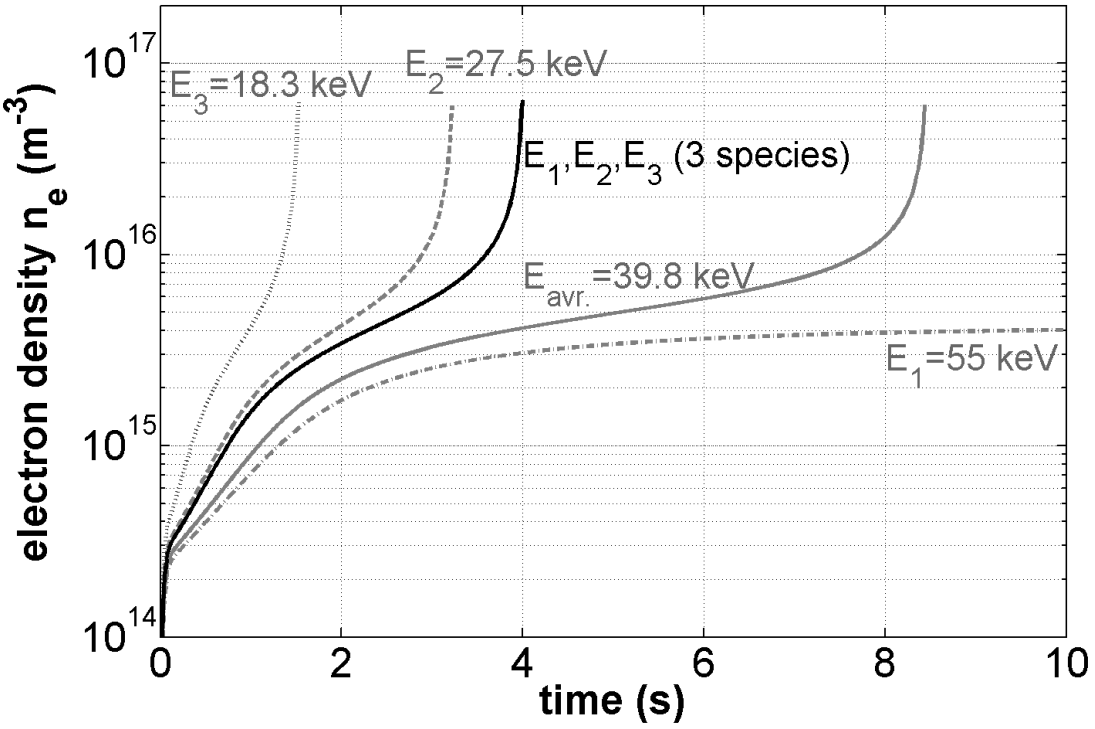

Figure 4. Temporal evolution of the electron density for a W7-X hydrogen plasma start-up simulated with three beam energies (black continuous line). The gray lines indicate plasma start-ups with mono-energetic beams ($E_{avr.} = \sum_j E_j \cdot p_j$, $E_1 = e \cdot U$, $E_2 = E_1/2$ and $E_3 = E_1/3$).

$E_2 = 27.5\,\mathrm{keV}$ and $E_3 = 18.3\,\mathrm{keV}$, plasma start-up occurs and the plasma start-up time decreases with decreasing energy. This result is in accordance with Ott [8], who also investigated the energy components of the neutral beam for W7-AS parameters. The most favorable beam energy concerning the start-up time is somewhere below $E_3 = 18.3\,\mathrm{keV}$. The reason for small beam energies being more advantageous for plasma start-up is the (energy-dependent) ionization and charge exchange atomic data (see sources stated in the Appendix). The non-linear energy dependence of the atomic collision cross-sections for beam-background gas reactions lead to a specific weighting of the reaction processes that cannot be resembled by energy averaging. With the most favorable beam energy below $E_3 = 18.3\,\mathrm{keV}$, this is why the beam energy resolved simulation calculates a faster start-up time.

A general decrease of the beam energies (by reducing the acceleration voltage U) is not possible without decreasing the neutral beam injection power due to the requirement to keep the perveance match for the neutral beam. When reducing the neutral beam power, the plasma start-up time becomes longer. This effect has been observed and investigated by Kaneko [9] and Ott [8]. Therefore, decreasing the neutral beam energy is not an option for decreasing the plasma start-up time.

3.4. Sensitivity of simulation results to cross-section data

In order to investigate the dependence of the plasma start-up time, denoted as τ_{psu}, on cross-section uncertainties, a variation of each considered cross-section value was made. The source of each cross-section is summarized in the Appendix. Figure 5 shows

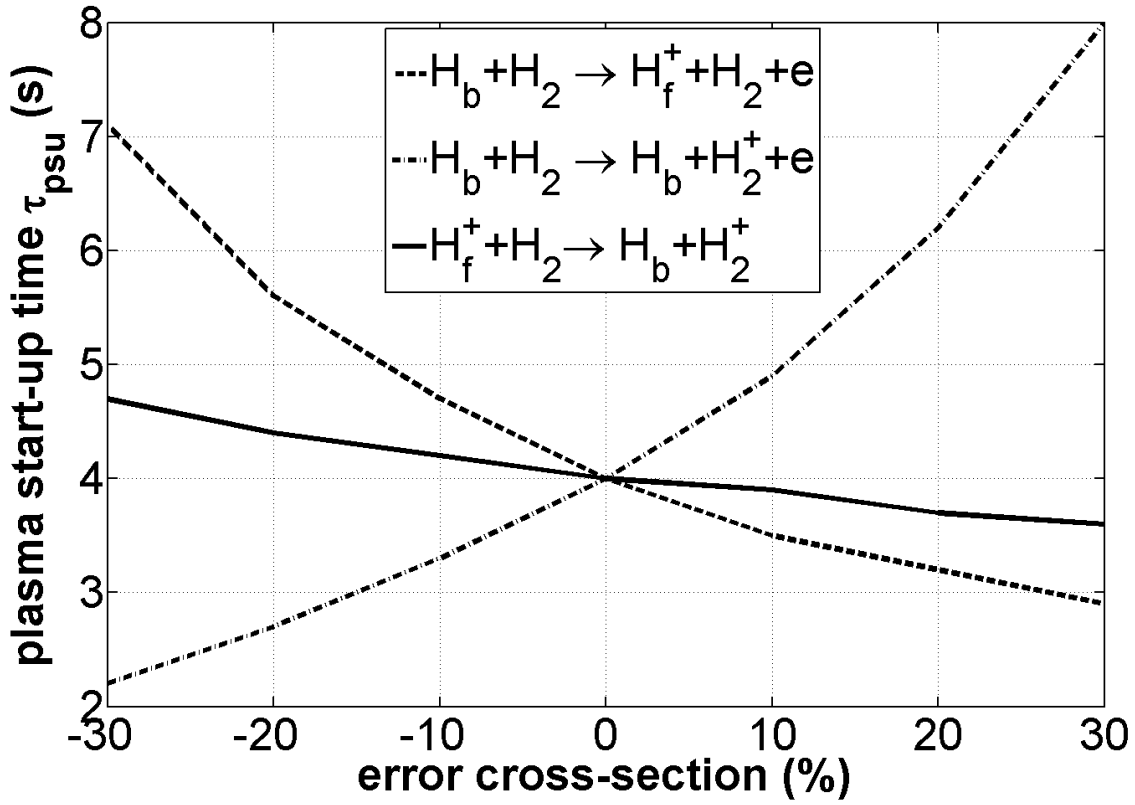

Figure 5. Dependence of the plasma start-up time τ_{psu} on variations of single cross-section values for a hydrogen beam in a pure hydrogen target.

variations for every cross-section with highest impact on τ_{psu}; all σ have been varied in steps of 10%. The simulated plasma start-up times are for the variation of one cross-section value each. It can be seen that the model is very sensitive to collisions between beam particles and neutral gas. A 30% error in certain cross-section values may lead to a deviation of τ_{psu} from -50% to +100%. It is relevant to consider these deviations, because some of the data sources indicate uncertainties of up to 50%.

3.5. W7-X plasma start-up in helium

By introducing three new rate equations (6)-(8), plasma start-up in helium was simulated for W7-X. The evolution of the helium species He, He^+ and He^{2+} as well as the neutral hydrogen density H_2 in a target of 50% helium and 50% hydrogen neutral gas is shown in Figure 6. The plasma start-up time drops significantly by adding helium

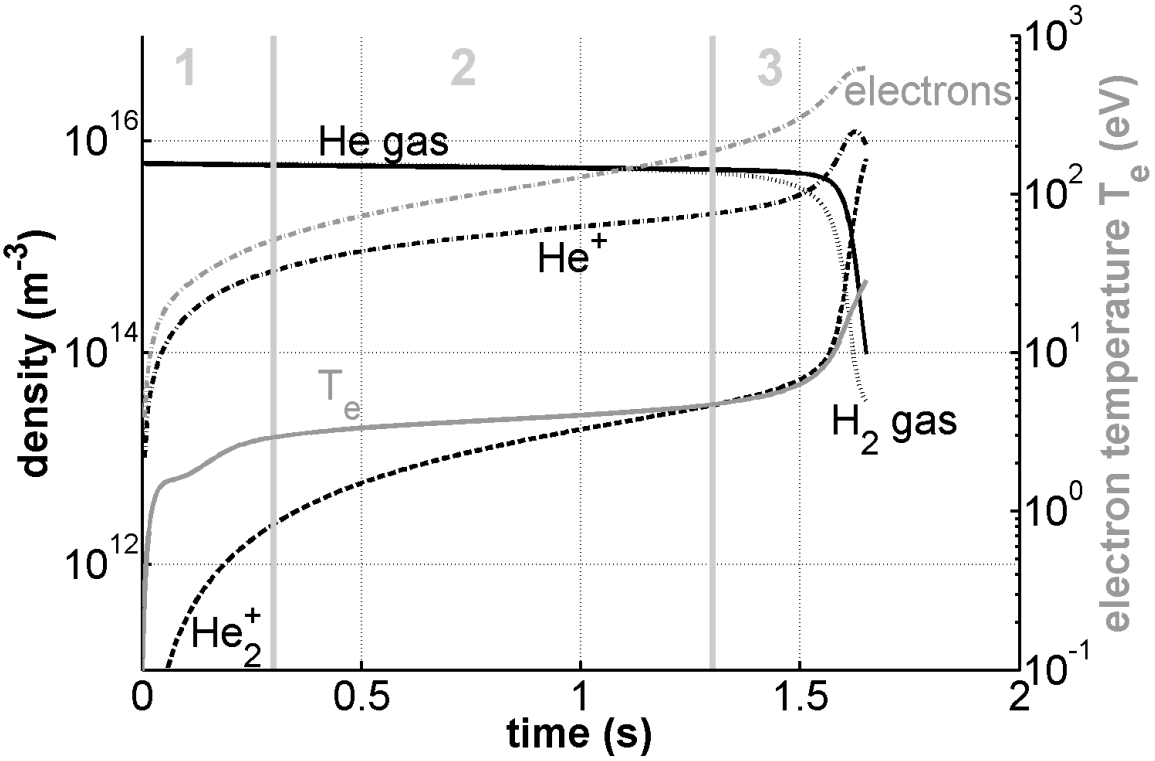

Figure 6. Temporal development of target particle densities during a plasma start-up in a neutral gas consisting of 50% helium and 50% hydrogen.

to the neutral gas. This is demonstrated in Figure 7, where the dependence of the start-up time on the admixture of helium with hydrogen is shown for a given neutral gas pressure, p_{gas}. Only for high helium fraction ($> 80\%$), τ_{psu} slightly increases.

To examine the role of helium in decreasing τ_{psu}, the temporal evolution of the electron temperature is shown for different hydrogen-helium admixtures in Figure 8. The electron temperature shortly after the beam switch on ($t = 0\,\mathrm{s}$) is higher for admixtures with higher helium fractions. This is due to the electron cooling rates (see Figure 2) that are considerably lower in helium compared to hydrogen for electron temperatures below 10 eV. Furthermore, the electron temperature minimum at $t \approx 0.1\,\mathrm{s}$ vanishes for higher helium fractions. The minimum is caused by the H_2^+ density, that increases strongly after the beam is switched on and cools the electrons. With decreasing hydrogen fraction, the H_2^+ density becomes smaller and the minimum vanishes.

Besides less electron cooling, there are also less electrons lost in helium gases, leading to a higher electron density. This is due to the absence of the dissociative recombination $e+H_2^+ \rightarrow 2H$. The dissociative recombination rate coefficient is approximately five orders of magnitude higher than for radiative recombination in either hydrogen or helium (see [15]).

However, the increase of τ_{psu} for helium fractions above 80% in Figure 7 indicates a disadvantage in helium, too. The favorable effects in helium are counterweighted by the high ionization thresholds of helium species (He: 24.6 eV, He^+: 54.4 eV.). This can

be observed in Figure 8. Although the electron temperatures are higher after beam switch on with rising helium fraction, the increase of the electron temperatures during the third phase (breakdown to plasma) becomes less steep. Ionization of hydrogen is initiated faster during the breakdown to plasma phase. This is confirmed in Figure 6, where a start-up in a target gas with equal hydrogen and helium share is simulated and the evolution of both neutral gas densities are shown.

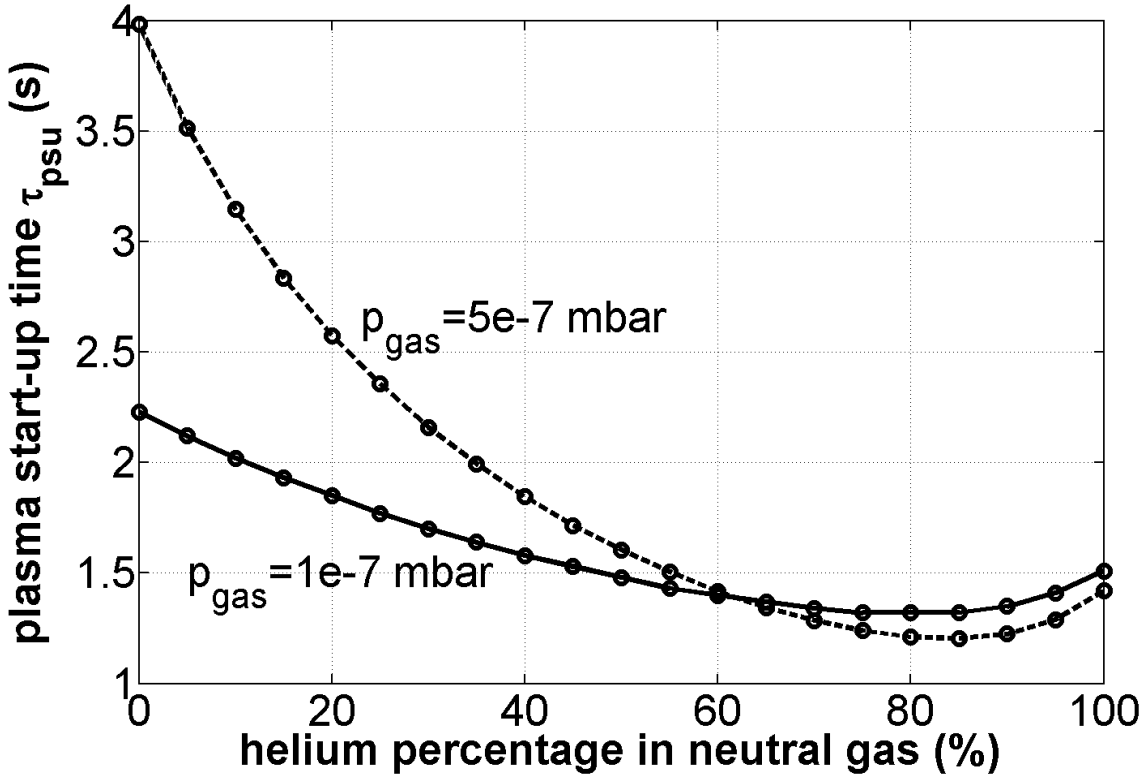

Figure 7. Start-up time (criteria: $T_e > 15\,\mathrm{eV}$) for different neutral target gas admixtures of He and H_2 in W7-X. The total neutral gas pressure p_{gas} was kept constant, but the partial pressures of He and H_2 have been varied.

3.6. Plasma start-up with deuterium beams

Table 2. Parameters planned for the W7-X deuterium beam operation [13].

beam power (2 sources)	P	4.8	MW
acceleration voltage	U	60	kV
beam species mix	p_j	72:20:8	

For plasma generation with deuterium beams it is found that there are some advantages, but also disadvantages for a plasma start-up compared to hydrogen beams. Plasma start-up with deuterium beams has the same characteristics to a start-up with

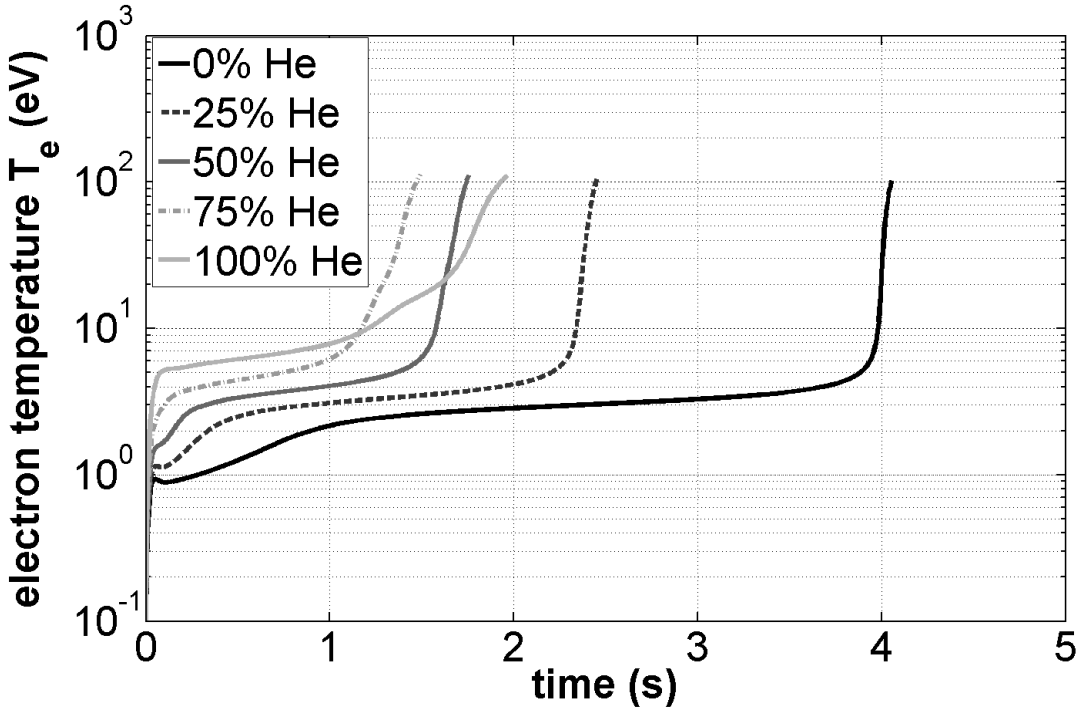

Figure 8. Temporal development of the electron temperature T_e for different partial pressures of He and H_2 (total neutral pressure was set constant).

a hydrogen beam because the same rate coefficient and cross-section collision data is used for isotopes of the same element [18]. In section 2 it was shown that lower beam energy per atomic mass unit is more favorable for reducing the plasma start-up time. In W7-X, deuterium beams have a lower beam energy (eV/amu) than hydrogen beams and therefore higher ionization cross-sections (see Table 2). However, the deuterium particles are slower for a given acceleration voltage, U. The interplay of both effects leads to decreased particle reaction rates

$$R = n_i \cdot n_j \cdot \sigma_{i,j} \cdot v \tag{14}$$

considered in the particle rate equations (2)-(10).

There are technical considerations being relevant to the assessment of deuterium operation. An advantage of deuterium operation is that deuterium beams in W7-X are operated at higher beam power than hydrogen beams [13]. Higher neutral beam powers are more favorable for the plasma start-up time. However, the distribution of the beam energy fractions, p_j, is more disadvantageous for τ_{psu}, since the full energy fraction E_1 is highest (see Table 2).

For the specific values considered in this comparison the factors roughly compensate each other. In total, the plasma start-up time with deuterium beams is essentially the same as for hydrogen beams in W7-X ($\tau_{psu}(\mathrm{D}) = 4.2\,\mathrm{s}$, $\tau_{psu}(\mathrm{H}) = 4\,\mathrm{s}$).

3.7. Parameter studies for W7-X

In order to assess the impact of external control parameters on the plasma start-up with neutral beam injection and to investigate how the plasma start-up in W7-X can be improved, parameter variations have been conducted. The background gas pressure, the initial electron density and the confinement times are analyzed in this section.

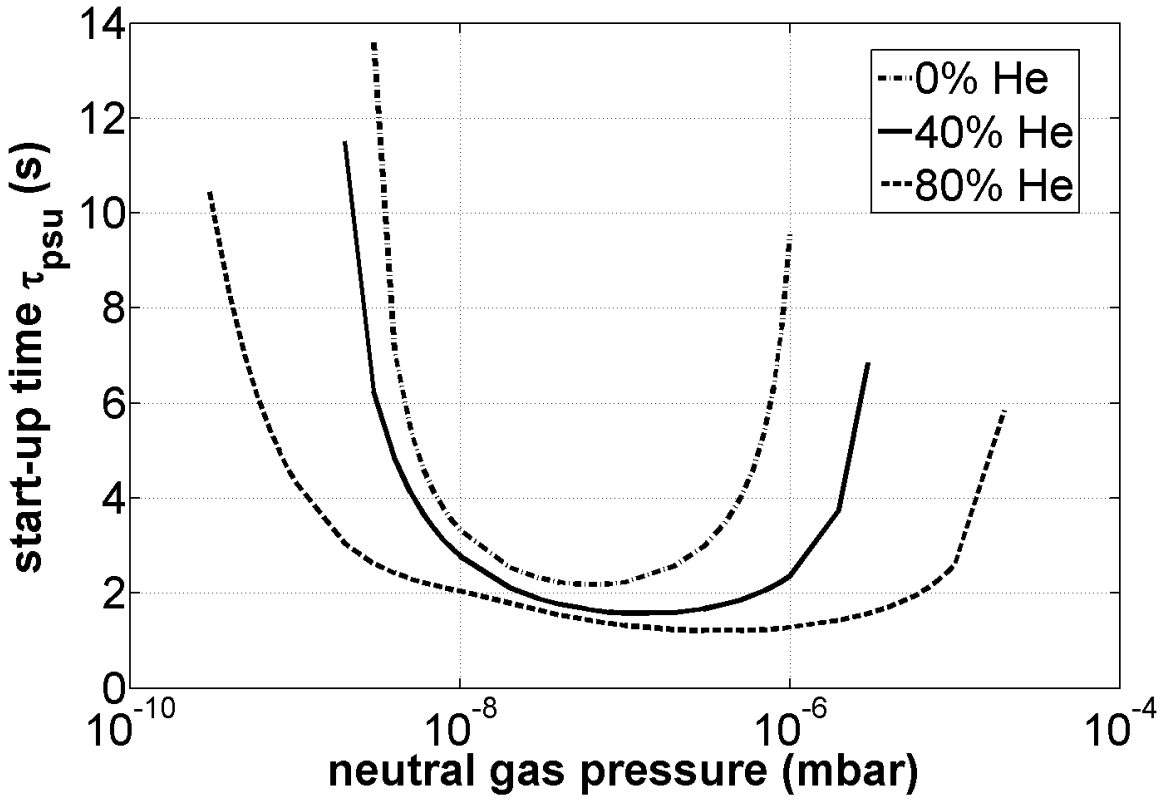

Figure 9. Plasma start-up time (criterion: $T_e > 15\,\mathrm{eV}$) in a pure hydrogen gas target and in a helium-hydrogen admixtures for different neutral gas pressures p_{gas}.

The neutral gas pressure determines the electron and ion densities reached during the start-up. But the higher the neutral gas pressure (and thus the neutral density), the higher the electron cooling (by inelastic collisions) and charge exchange with the ionized beam particles. Therefore, an optimal neutral gas pressure exists for the plasma start-up.

Figure 9 displays the variation of the initial neutral gas pressure, p_{gas}, with respect to the plasma start-up time, τ_{psu}. The output of the model is given for a pure hydrogen target gas and two helium-hydrogen admixtures. In all cases a minimum plasma start-up time has been found, broadened by the admixture of helium. τ_{psu} increases for neutral gas pressures above the minimum values because the electrons are cooled due to an increased rate of inelastic collisions with the neutral gas. Above a pressure of

10^{-6} mbar, there is no plasma start-up in W7-X in pure hydrogen targets (standard parameters) due to cooling. In helium admixtures, the upper pressure limit increases to 10^{-5} mbar because less electron cooling and recombination take place. However, for low pressures, τ_{psu} increases because both electron and ion generation become limited by the density of the neutral gas. The dependence of the plasma start-up time on the neutral gas pressure apparently resembles the characteristic of the Paschen curve, but its physical origins are different. The Paschen curve denotes the discharge voltage in a gas between parallel plates over the neutral gas pressure times the distance of the plates [19].

It is not possible in experiments such as W7-X to reach the lower pressure limits in Figure 9. However it was decided to display these values in order to illustrate the Paschen-like shape of the curves.

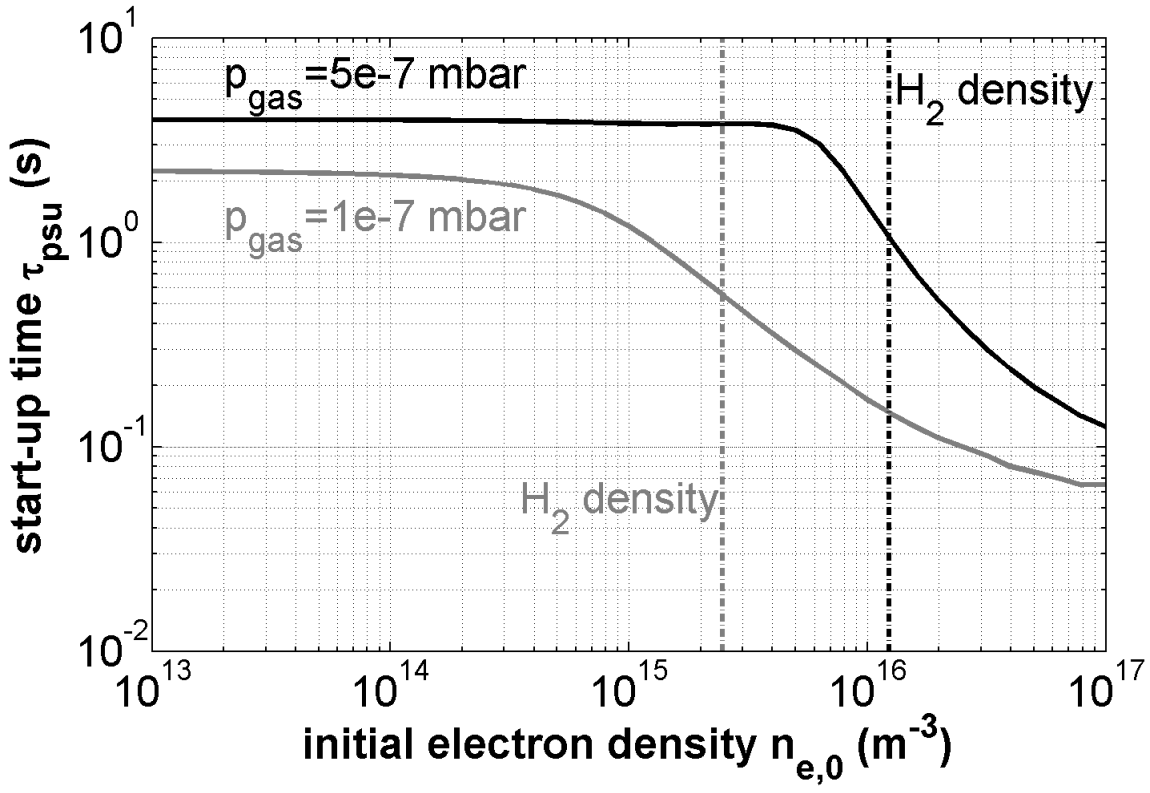

Figure 10. Start-up time (criterion: $T_e > 15\,\mathrm{eV}$) in dependence on the initial electron density, $n_{e,0}$, (the initial ion density was set equal to the electron density). The vertical lines indicate the initial neutral gas density during the simulation.

Due to the significance of the electrons during the plasma start-up, pre-ionization was investigated for W7-X as an option to improve the plasma start-up time. In Figure 10 it can be seen that τ_{psu} begins to decrease for a pre-beam electron (and ion) density of $n_{e,0} = 4 \cdot 10^{15}\,\mathrm{m}^{-3}$. The standard H_2 gas pressure of $p_{gas} = 5 \cdot 10^{-7}$ mbar is equivalent to a neutral gas density of $1.2 \cdot 10^{16}\,\mathrm{m}^{-3}$ (assuming room temperature). Thus, pre-beam ionization begins to show an effect on τ_{psu} (given the standard neutral gas pressure)

for an ionization grade of 25%. For lower neutral gas densities, the effect begins for lower ionization grades. A plasma start-up time of $\tau_{psu} = 0.4\,\mathrm{s}$ could be reached with an ionization grade of 66% in W7-X ($p_{gas} = 5 \cdot 10^{-7}\,\mathrm{mbar}$). This means a greater initial electron than neutral density before the plasma start-up. Again, for lower pressures, the ionization grade necessary for $\tau_{psu} = 0.4\,\mathrm{s}$ drops, but remains high. One way to achieve these ionization grades could be e.g. by 2.45 GHz microwaves, as in Heliotron J [7].

Furthermore, the fast ion and the thermal ion-confinement times, τ_f and τ_{th}, have been varied to estimate their effect for the plasma start-up time. With the thermal ion density higher than the fast beam ion density, the start-up time is more strongly dependent on τ_{th} than on τ_f. For decreasing the standard value of $\tau_{th} = 1\,\mathrm{s}$ to $0.4\,\mathrm{s}$, the plasma start-up time is increasing and, for $\tau_{th} < 0.4\,\mathrm{s}$, no plasma start-up is expected for W7-X. The thermal ion-confinement time can be interpreted as perpendicular particle transport of thermal ions and electrons. Perpendicular transport is assumed to be dominated by anomalous Bohm-diffusion [20] as a worst case during the plasma start-up:

$$\tau_{th} = \frac{16 B a_{min}^2}{2 T_e} \tag{15}$$

where B is the poloidal magnetic field strength in Tesla and a_{min} is the minor radius of the magnetic fusion device. With Equation (15), a thermal confinement time $\tau_{th} < 0.4\,\mathrm{s}$ translates to a magnetic field strength of $B < 0.7\,\mathrm{T}$ for W7-X ($a_{min} = 0.53\,\mathrm{m}$, $T_e = 4\,\mathrm{eV}$). The standard thermal ion-confinement time $\tau_{th} = 1\,\mathrm{s}$ is equivalent to a magnetic field strength of $B = 1.8\,\mathrm{T}$. The fast ion-confinement time begins to have an effect on τ_{psu} if $\tau_f > 0.1\,\mathrm{s}$.

4. Experimental validation of the model

In order to assess the outcome of the presented model, a comparison was made between simulated and experimental data from Wendelstein 7-AS (W7-AS) and the Large Helical Device (LHD). Afterwards, the beam-interaction length, l, is varied to evaluate its influence on the plasma start-up time.

4.1. W7-AS data

In order to validate the plasma start-up in W7-AS, experimental data from the W7-AS databank and also from [8] was used. The same shot (47682) as in [8] is analyzed in this paper. This shot was shortly taken after a cleaning discharge. Figure 11 compares the simulated and the measured electron densities during the plasma start-up phase. Since no measurements of the neutral gas pressure were available in the W7-AS databank, neutral gas pressures with good agreement to the experimental electron density was searched. In Figure 11 the neutral gas values with best agreement are presented.

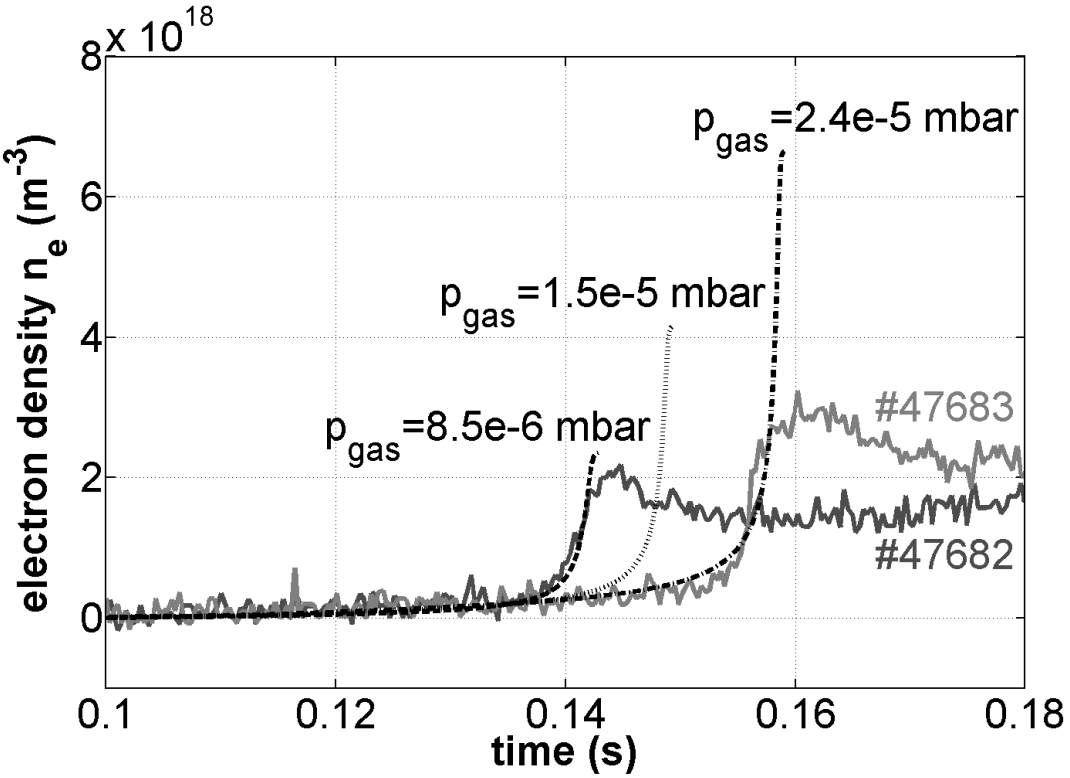

Figure 11. Temporal evolution of measured (continuous) and simulated (dotted curves) mean electron density. A line-integrated electron density was measured by a microwave interferometer. The interferometer signal had to be divided by the effective path length (20 cm) of the measurement in the plasma for comparison with the simulated electron density. The NBI started at $t = 0.1\,\mathrm{s}$ at a power of 1.6 MW.

The neutral pressure prior to the NBI pulse depends on the prefill gas flux, the pumping speed (main pumps and NBI Titanium sublimation pumps) and the condition of the wall. The prefill gas flux could also not be accessed in the databank because data was missing for the gas flux valve used during the investigated shots. However, it is assumed that the neutral gas pressure was relatively low and in the order of 10^{-5} mbar, estimated from the prefill gas settings noted in the shot protocols.

A plasma start-up time of approximately $\tau_{psu} = 40\,\mathrm{ms}$ was found experimentally for shot 47682. In this case, τ_{psu} is defined as the time-point of exponential increase of electron density that coincides with the strong increase of the electron temperature around $T_e = 10\,\mathrm{eV}$ (see section 3.2). In the next shot, although all conditions were kept the same, the plasma start-up time was found to be $\tau_{psu} = 55\,\mathrm{ms}$. The delay was assumed to be caused by the higher neutral background gas pressure. Hydrogen saturation of the wall and higher wall recycling fluxes may explain an increase of neutral gas pressure.

The neutral gas pressures assumed for the simulations are relatively low compared with ECRH-driven plasma start-ups. For plasma start-up with NBI only, prefill of neutral gas had to be managed carefully in W7-AS [4]. Only for low neutral gas densities, successful plasma start-up could be observed. If neutral gas prefill was too long (leading

to high neutral gas pressure), no plasma start-up occurred.
With the model it was possible to find very good agreement with the experimental results for neutral gas pressures of $p_{gas} = 8.5 \cdot 10^{-6}$ mbar (47682) and $p_{gas} = 2.4 \cdot 10^{-5}$ mbar (47683). These values are in the order of the estimated value of the neutral gas pressure. For shot 47682, there is also good agreement of the simulation with the maximum electron density reached after the start-up phase. It is noted that the model is not considered to fit reality after plasma start-up due to its 0-dimensional aspect.
In Figure 11, the simulation with a pressure of $p_{gas} = 1.5 \cdot 10^{-5}$ mbar was included to allow comparison with Otts fit in [8]. Ott did fit shot 47682 with a good agreement, indicating that his model simulated faster plasma start-ups for the same neutral gas pressure as the model presented in this paper. This was unexpected, as Otts model uses an averaged beam energy (see section 2.1) and therefore should generate a higher start-up time. The reason for his model simulating faster start-up times (for the same input parameters) was found to be the H_2^+ electron cooling rate. It was considered for the model in this paper, but not by Ott.
A different explanation of the delay are impurities. Impurities are considered to increase with every NBI-heated discharge. Impurities cause a delay of the plasma start-up due to electron cooling (see section 2.3). For all W7-AS simulations, the input parameters

Table 3. Standard parameters used for W7-AS simulations.

interaction length*	l	2	m
plasma volume	V_p	1.25	m^3
vessel volume	V_v	7	m^3
thermal ion-confinement time*	τ_{th}	0.1	s
fast ion-confinement time*	τ_f	0.01	s
initial electron temperature*	$T_{e,0}$	1	eV
gas temperature	T_{gas}	293	K
beam power (4 sources)	P	1.6	MW
acceleration voltage	U	50	kV
beam species mix	p_j	35:37:28	

were set as noted in Table 3.

4.2. LHD data

Plasma start-up with NBI alone has been demonstrated and analyzed very early in LHD [9]. In this paper, recent shots have been analyzed with regard to the plasma start-up time. In Table 4, two neutral beam calibration shots are presented where each of the neutral beams were injected separately. Although it was not intended to generate a plasma in these shots, plasma was generated by the tangential neutral beams nonetheless, presumably due to the low neutral gas pressure in the device. Several far-infrared interferometers measured the line-integrated electron density during plasma

generation at different positions in the LHD vessel. The electron density reached values of up to $10^{19}\,\mathrm{m}^{-3}$. The plasma start-up time was derived from the average of all interferometers signals, as plasma generation (indicated by the sharp increase of electron density) was measured with some ms delay in some interferometers.

Table 4. Beam parameters and plasma start-up time measured during neutral beam port-through power calibration shots in the LHD. A comparison was made with the simulated plasma start-up time.

Shot	NB#	beam energy	beam power	neutral pressure	τ_{psu} measured	τ_{psu} simulated	deviation
119496	3	170 keV	4.2 MW	2.5e-5 mbar	0.17 s	0.175 s	+3%
119496	1	185 keV	4.6 MW	2.9e-5 mbar	0.10 s	0.133 s	+33%
123150	3	178 keV	4.7 MW	1.9e-5 mbar	0.09 s	0.117 s	+30%
123150	1	190 keV	5.2 MW	2.3e-5 mbar	0.04 s	0.094 s	+135%

Due to the 0-dimensional aspect of the model, an average was also taken from the five operating pressure gauges during the shots. It was observed that the gauges did measure different - though similar - neutral pressures, depending on their position in the LHD. The averaged neutral pressure values during neutral beam power switch on are listed in Table 4. The values listed in Tables 4 and 5 were used as input parameters for the simulations. There was a good and reasonable agreement between the measured and the simulated plasma start-up times, except for the last plasma generation. A detailed assessment of this case did not lead to a satisfactory explanation for the difference between experimental findings and simulations.

Table 5. Standard parameters used for LHD simulations.

interaction length*	l	5.6	m
plasma volume	V_p	27	m^3
vessel volume	V_v	210	m^3
thermal ion-confinement time*	τ_{th}	1	s
fast ion-confinement time*	τ_f	0.1	s
initial electron temperature*	$T_{e,0}$	1	eV
gas temperature	T_{gas}	293	K
beam power	P	see Table 4	
acceleration voltage	U	see Table 4	
beam species mix	p_j	100:0:0	

4.3. Variation of beam-plasma interaction length

In comparison to W7-AS or LHD (see section 4), plasma start-up in W7-X is expected to take significantly longer. This is primarily due to the ratio of the beam-plasma interaction length l and the plasma volume, V_p. An overview of these quantities for each device is given in Table 6.

Table 6. Beam plasma interaction length (l), plasma volume (V_p) and ratio (l/V_p) for W7-X, LHD and W7-AS.

	l (m)	V_P (m^3)	l/V_P (m^{-2})
W7-X	0.6	30	0.02
LHD	5.6	27	0.21
W7-AS	2	1.25	1.6

W7-X has not only the largest plasma volume, but also the shortest beam-interaction length. Therefore, the ratio l/V_p is smallest in W7-X and e.g. two orders of magnitude smaller than in W7-AS. This explains why the plasma start-up time is two orders of magnitude higher in W7-X ($\tau_{psu} = 4\,\mathrm{s}$) than in W7-AS ($\tau_{psu} = 0.04\,\mathrm{s}$).

In order to assess τ_{psu} for different beam-plasma interaction lengths, l was varied

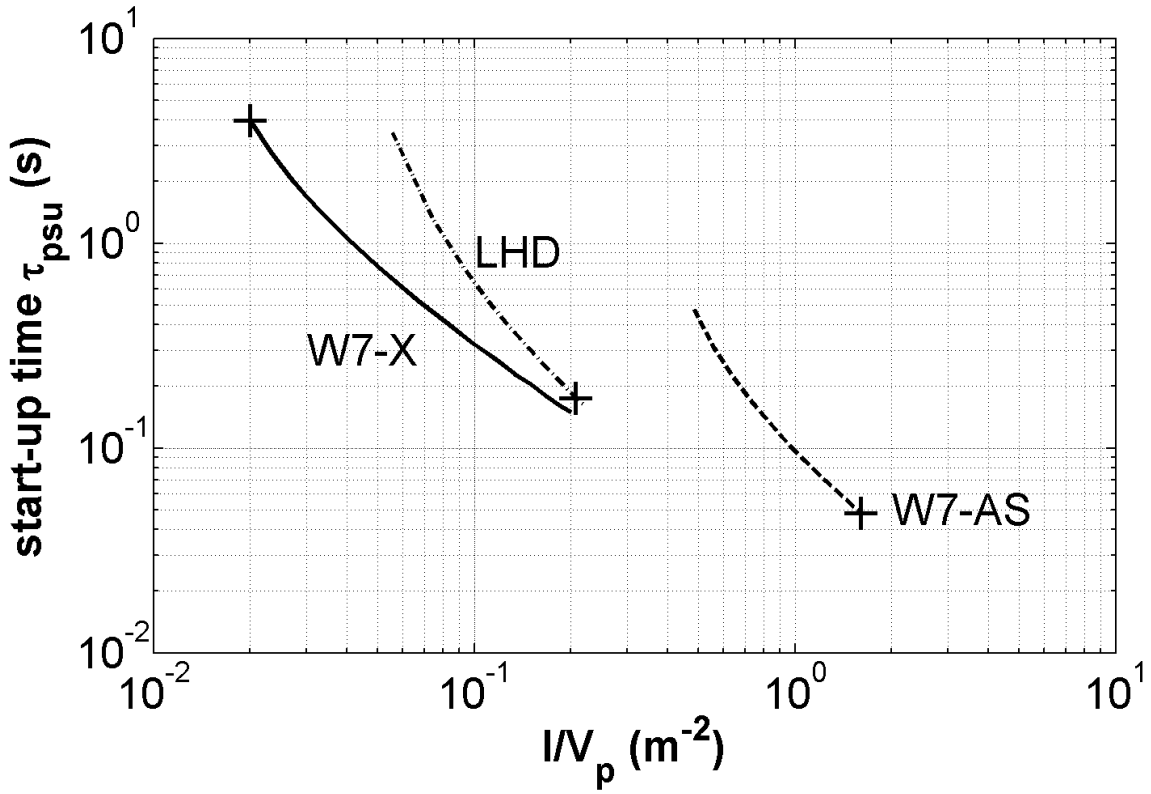

Figure 12. Start-up time (criterion: $T_e > 15\,\mathrm{eV}$) for varying ratio l/V_p in W7-X, W7-AS and LHD. The cross markers indicate the l/V_p ratios for the actual configurations of each device. W7-X parameters: see Table 1. W7-AS and LHD: parameters listed in Tables 3 and 5.

between 0.5 m to 6 m in LHD and W7-X and from 0.5 m to 2.5 m in W7-AS in Figure 12. Due to different neutral gas densities, plasma volumes and neutral beam quantities, the variation does not calculate the same start-up times for the same l/V_p-ratio values in the machines. For W7-X, the model calculates that the plasma start-up time decreases

to $\tau_{psu} = 0.4\,\mathrm{s}$ for an beam-target interaction length of $l = 2.4\,\mathrm{m}$. For the same l/V_p-ratio values, LHD has higher plasma start-up times τ_{psu} due to higher neutral gas pressures ($p_{gas} = 2.5{\cdot}10^{-5}\,\mathrm{mbar}$) than in W7-X ($p_{gas} = 5{\cdot}10^{-7}\,\mathrm{mbar}$). For W7-AS, the variation of l resulted in smaller l/V_p-ratios due to the relatively small plasma volume of the device.

5. Summary and Conclusions

The plasma start-up with neutral beam injection (NBI) for the stellarator Wendelstein 7-X has been investigated. To simulate plasma start-up in a stellarator, a 0-dimensional model expanding the models by Ott [8] and Kaneko [9] was used to evaluate the particle reaction rates and the electron temperature changes during the plasma start-up.
Three major expansions were made to the model for the approach of plasma generation in W7-X:

- First the energy components of the positive ion beam were considered by three fast ion equations instead of one for positive NBI. The energy resolved model shows a lower value of start-up time than an averaged beam energy since the low energy E_2, E_3 components are more effective in ionizing the neutral gas.
- The second extension was to allow helium for admixtures to the particle balances. For W7-X, helium admixtures result in a considerable decrease of the plasma start-up time due to the absence of dissociative processes in helium. Dissociative processes are disadvantageous for plasma start-up in general due to high rate coefficients at low energies, resulting in high electron cooling rates for electron temperatures $T_e < 10\,\mathrm{eV}$. Moreover, fewer electrons are lost due to the absence of dissociative recombination in helium.
- The third change to the model was the inclusion of deuterium beams. For deuterium beam operation, no essential improvement of plasma start-up was found because of two counter-acting effects. On the one side, deuterium beams have higher power and higher cross-sections. Both effects decrease the plasma start-up time. On the other side, deuterium beam particles have a slower velocity due to their increased mass and this reduces the particle reaction rates.

To assess the accuracy of the simulations, comparison with experiments has been performed. The plasma start-up times determined by the model have been found to be in good agreement with LHD data, except for one plasma generation. It was observed that all simulated start-up times were larger than the measured ones. The validation with W7-AS data was hampered by the fact that the neutral gas pressure during the experiment could not be accessed. For W7-AS, the plasma start-up time could be fitted with a very good agreement to the start-up time. However, the fitted neutral gas pressure value was only half as high as stated by Ott [8]. For the pressure value stated by Ott, the simulated start-up time was $\approx +20\%$ above the measured one.
In conclusion, the neutral gas pressure has been found to be a crucial input parameter for the plasma start-up model. It is assumed that the model calculates the plasma

start-up time in the correct order of magnitude, but with a tendency of simulating longer start-up times than measured. The deviation is probably caused by the applied cross-sections. An investigation of the relation between the start-up time and cross-section errors stated in the literary sources showed that 30% errors for certain cross-section values can cause deviations of the start-up time of ±50%.

For W7-X, a plasma start-up time of $\tau_{psu} \approx 4\,\mathrm{s}$ was determined by the model for a set of standard parameters and the NBI geometry as planned for initial operation (nearly perpendicular injection). Since no impurities are considered in the model, this time is only accurate for a start-up with a negligible amount of impurities. The neutral beam operation time necessary for plasma start-up clearly exceeds the allowed neutral beam operation time of 400 ms. The time-limitation of neutral beam operation is due to the heat load of the tiles opposite to the neutral beam entrance. In order to reduce the start-up time of W7-X, three options have been found: Two are the addition of seed electrons and helium in the target gas. As an example, an ionization grade of 33% (generated with additional heating sources) and a hydrogen/helium admixture of 20%/80% could lower the start-up time to $\tau_{psu} = 0.6\,\mathrm{s}$. A third and more effective option would be to use another neutral beam port with a tangential injection angle. Simulations in this study show that plasma start-up in W7-X takes significantly longer as in W7-AS or LHD, where tangential NBI operation is used. The key parameter to explain this is the ratio of interaction length, l, and plasma volume, V_p. The quantity l/V_p is the primary driver for the plasma start-up time. In addition, due to the low l/V_p ratio, plasma start-up in W7-X can only be achieved for relatively low neutral gas pressures. This is why a pressure of $p_{gas} = 5 \cdot 10^{-7}\,\mathrm{mbar}$ was chosen for simulations presented in this study. This value is significantly lower than the pressures operated in W7-AS and LHD, where start-up could be initiated at about $10^{-5}\,\mathrm{mbar}$.
In W7-X, a plasma start-up time of $\tau_{psu} < 0.4\,\mathrm{s}$ could be achieved for a beam interaction length of $l > 2.4\,\mathrm{m}$ for the set of standard parameters. Additionally, the time-limit for the beam operation is expected to be higher in a more tangential geometry. From the design point of view, there are other ports allowing a more tangential NBI operation in W7-X. However, to use these ports would require the modification of the existing injector boxes. The resources for this are not available.

Acknowledgments

The corresponding author gratefully acknowledges the fruitful correspondences with T. Wauters on the derivation of the rate coefficient as defined in [15] and with D. Wünderlich on the application of atomic data for different isotopes.
The authors appreciate the work and support of the experimental team of LHD for the provided plasma start-up data.

Appendix

Collisions between the beam and hydrogen particles are given in table 7 and those between the beam and helium particles in table 8. The dependence of reaction rate coefficients involving hydrogen species on electron temperature is shown in figure 13.

Table 7. Collisions between beam and hydrogen particles.

reaction	symbol	source
$H_b + e \rightarrow H_f^+ + 2e$	$\left\langle \sigma_{e,b}^{ion.} \cdot \lvert v_f - v_e \rvert \right\rangle$	[15] 2.1.5
$H_b + H^+ \rightarrow H_f^+ + H$	$\sigma_{1,b}^{cx}$	[21] A-22
$H_b + H^+ \rightarrow H_f^+ + H^+ + e$	$\sigma_{1,b}^{ion.}$	[15] 3.1.6 & [21] D-6
$H_b + H_2^+ \rightarrow H_f^+ + H_2$	$\sigma_{2,b}^{cx}$	[21] A-22 & [22]
$H_b + H_2^+ \rightarrow H_f^+ + H_2^+ + e$	$\sigma_{2,b}^{ion.}$	[22]
$H_b + H_2 \rightarrow H_f^+ + H_2 + e$	$\sigma_{g,b}^{ion.}$	[21] E-6
$H_f^+ + H_2 \rightarrow H_b + H_2^+$	$\sigma_{f,g}^{cx}$	[21] A-28
$e + H_2 \rightarrow H_2^+ + 2e$	$\left\langle \sigma_{e,g}^{ion.} \cdot v_e \right\rangle$	[15] 2.2.9
$H_b + H_2 \rightarrow H_b + H_2^+ + e$	$\sigma_{b,g}^{ion.}$	[21] D-4
$H_f^+ + H_2 \rightarrow H_f^+ + H_2^+ + e$	$\sigma_{f,g}^{ion.}$	[21] D-16
$e + H_2^+ \rightarrow 2H$	$\left\langle \sigma_{e,2}^{rec.} \cdot v_e \right\rangle$	[15] 2.2.14
$e + H_2^+ \rightarrow H^+ + H + e$	$\left\langle \sigma_{e,2}^{dis.} \cdot v_e \right\rangle$	[15] 2.2.12
$e + H^+ \rightarrow H + h\nu$	$\left\langle \sigma_{e,1}^{rec.} \cdot v_e \right\rangle$	[15] 2.1.8

Table 8. Collisions between beam and helium particles.

reaction	symbol	source
$H_b + He \rightarrow H_f^+ + He + e$	$\sigma_{He,b}^{ion.}$	[21] E-10
$H_b + He^+ \rightarrow H_f^+ + He^+ + e$	$\sigma_{He^+,b}^{ion.}$	[21] D-72
$H_b + He^+ \rightarrow H_f^+ + He$	$\sigma_{He^+,b}^{cx}$	[21] A-62
$H_b + He^{2+} \rightarrow H_f^+ + He^{2+} + e$	$\sigma_{He^{2+},b}^{ion.}$	[15] 6.1.3 & [21] D-96
$H_f^+ + He^+ \rightarrow H_b + He^{2+}$	σ_{f,He^+}^{cx}	[21] A-54
$H_f^+ + He \rightarrow H_b + He^+$	$\sigma_{f,He}^{cx}$	[21] A-32
$e + He \rightarrow He^+ + 2e$	$\left\langle \sigma_{e,He}^{ion.} \cdot v_e \right\rangle$	[15] 2.3.9
$H_b + He \rightarrow H_b + He^+ + e$	$\sigma_{b,He}^{ion.}$	[21] E-16
$H_f^+ + He \rightarrow H_f^+ + He^+ + e$	$\sigma_{f,He}^{ion.}$	[21] D-24
$H_b + He^{2+} \rightarrow H_f^+ + He^+$	$\sigma_{b,He^{2+}}^{cx}$	[21] A-88
$e + He^{2+} \rightarrow He^+ + h\nu$	$\left\langle \sigma_{e,He^{2+}}^{rec.} \cdot v_e \right\rangle$	[15] 2.3.21
$e + He^+ \rightarrow He + h\nu$	$\left\langle \sigma_{e,He^+}^{rec.} \cdot v_e \right\rangle$	[15] 2.3.13
$e + He^+ \rightarrow He^{2+} + 2e$	$\left\langle \sigma_{e,He^+}^{ion.} \cdot v_e \right\rangle$	[15] 2.3.19
$H_b + He^+ \rightarrow H_b + He^{2+} + e$	$\sigma_{b,He^+}^{ion.}$	[21] E-28
$H_f^+ + He^+ \rightarrow H_f^+ + He^{2+} + e$	$\sigma_{f,He^+}^{ion.}$	[21] D-50

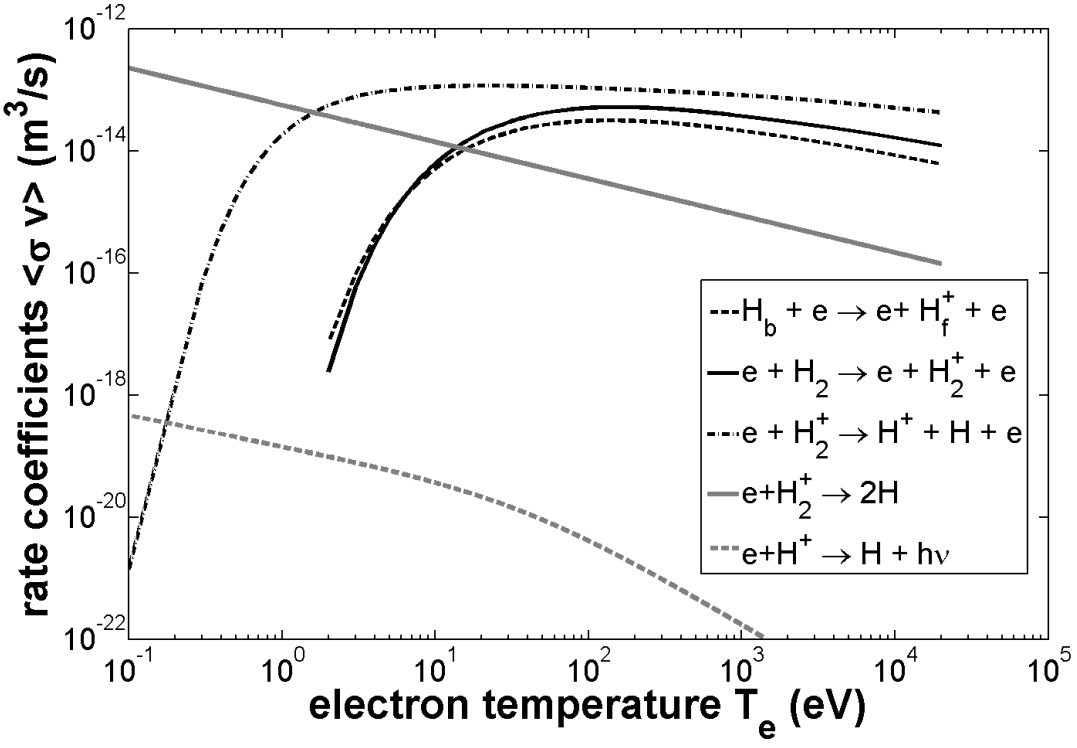

Figure 13. Dependence of reaction rate coefficients involving hydrogen species over electron temperature T_e. Ionization rate coefficients are colored black, recombination coefficients in gray.

References

[1] Cappa A., Castejon F., Tabares F.L. and Tafalla D. 2001 *Nucl. Fusion* **41** 363–74

[2] Talmadge J.N. and Anderson D.T. 1988 *Nucl. Fusion* **28** 1879

[3] Rust N., Heinemann B., Mendelevitch B., Peacock A. and Smirnov M. 2011 *Fusion Eng. Des.* **86** 728–31

[4] Ott W., Hartmann D., Penningsfeld F.-P. and Speth E. 2000 *27th EPS Conference on Contr. Fusion and Plasma Phys. (Budapest, Hungary)* vol 24B (European Physical Society) p 1617 http://epsppd.epfl.ch/Buda/pdf/p4_103.pdf

[5] Kaneko O. *et al* 1999 *Nucl. Fusion* **39** 1087–90

[6] Tabares F.L., Ascasibar E., Blanco E., Medina F., Pastor I. and Tafalla D. 2014 *Stellarator News* **144** 1–3

[7] Kobayashi S. *et al* 2011 *Nucl. Fusion* **51** 062002

[8] Ott W., Speth E. and the W7-AS Team 2002 *Nucl. Fusion* **42** 796-804

[9] Kaneko O., Takeiri Y., Tsumori K., Oka Y., Osakabe M., Ikeda K. and the LHD Experimental Group 2002 *Nucl. Fusion* **42** 441–7

[10] Fujimoto T., McWhirter R. 1990 *Phys. Rev. A* **42** 6588–601

[11] Speth E. 1989 *Rep. Prog. Phys.* **52** 57-121

[12] Kim H., Fundamenski W., Sips A. and EFDA-JET Contributors 2012 *Nucl. Fusion* **52** 103016

[13] McNeely P. *et al* 2013 *Fusion Eng. Des.* **88** 1034-7

[14] Miyamoto K. 1980 *Plasma Physics for Nuclear Fusion* (Cambridge, MA: MIT Press) p 90

[15] Janev R., Langer W., Evans K. and Post D. 1987 *Elementary Processes in Hydrogen-Helium Plasmas* (Berlin: Springer)

[16] Marchand R., Illescas C., Bonnin X. and Botero J. 1995 Radiative losses and electron cooling rates of hydrogen, helium, carbon and oxygen *Report* INDC(NDS)-309 International Nuclear Data Committee
[17] Hiskes J. 1962 *Nucl. Fusion* **2** 38-48
[18] Phaneuf R. 1992 *Atomic and Plasma-Material Interaction Data for Fusion* vol 2 (Vienna: IAEA) pp 75-90
[19] Wiesemann K. 1976 *Einführung in die Gaselektronik* (*Teubner Studienbucher Physik*) (Stuttgart: B.G. Teubner) p 48 (in German)
[20] de la Cal E. 2006 *Plasma Phys. Control. Fusion* **48** 1455-68
[21] Barnett C., Phaneuf R., Hunter H. and Kirkpatrick M. 1990 *Collisions of H, H_2, He and Li Atoms and Ions with Atoms and Molecules (ORNL-6086 V1)* (Oak Ridge, TN: Controlled Fusion Atomic Data Center)
[22] McCartney P., McGrath C., McConkey J., Shah M. and Geddes J. 1999 *J. Phys. B: At. Mol. Opt. Phys.* **32** 5103-8